Electrothermal Analysis of Breakdown in Carbon Nanofiber Interconnects

Toshishige Yamada, *Member, IEEE*, Tsutomu Saito, Drazen Fabris, and Cary Y. Yang, *Fellow, IEEE*

***Abstract*—To elucidate the observed current capacity behavior, a model is developed that takes into account heat transport through the entire carbon nanofiber interconnect test structure and breakdown location. The model also includes variations in contact location with the support material. The resulting predicted heat dissipation and current capacity are completely consistent with experimental data.**

***Index Terms*—Breakdown, carbon nanofiber (CNF), heat dissipation, maximum current density.**

I. Introduction

CARBON nanostructures have been studied for future interconnect applications due to their immunity to electromigration and excellent electrical and thermal transport properties [1]–[10]. Carbon nanofiber (CNF) is an allotrope of carbon nanotube (CNT) with a conelike central core structure and a multilayer outer wall structure (similar to multiwall CNT). However, unlike multiwall CNT, CNF does not have a hollow interior. To understand their transport properties as interconnects, we have developed a simple model based on measurements of the maximum current density $J_{\max}$ at breakdown [11], [12]. Furthermore, an imaging technique has been developed to quantify the observations [13]. Previous work [11] has indicated reasonable convergence of $J_{\max}$ data for CNFs suspended between two electrodes, while CNFs in partial contact with a SiO_2 substrate show larger $J_{\max}$ and wider scatter, as shown in Fig. 1. Since breakdown has been shown to be associated with the peak CNF temperature [6], [14], [15], substrate contact should enhance heat dissipation, increase the immunity to Joule heating, and hence increase $J_{\max}$. In this letter, we extend the previous model to capture the variation in heat transport to the SiO_2 substrate due to partial CNF contact. In addition, we demonstrate the contrast between heat dissipation through two different electrodes and through the substrate.

The new model adds two important parameters. One is the support fraction S, which is defined as the ratio of the length in contact with the SiO_2 substrate to the CNF interelectrode length L. S is measurable from a scanning electron microscope (SEM) image, where suspended segments are brighter due to more efficient secondary electron generation [13], as shown in Fig. 2. The other is the spatially varying heat dissipation factor

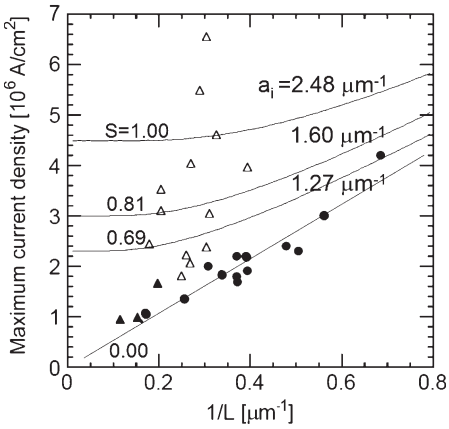

Fig. 1. Measured maximum current density $J_{\max}$ as a function of reciprocal CNF length L with different electrodes: (solid circles) suspended CNFs with Au electrodes and (solid triangles) suspended or (open triangles) SiO_2-supported CNFs with W–Au electrodes [12]. The lines indicate the calculated $J_{\max}$ from (2) for three fitting values of dissipation factor a_i with $R \ll 1$. Each line is labeled with the measured fraction of total supported segments S.

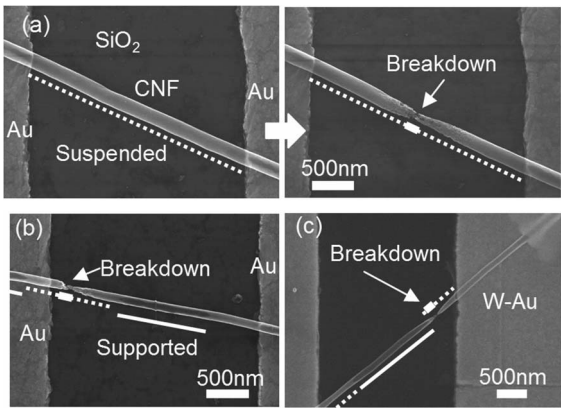

Fig. 2. Breakdown cases, where the dotted (solid) lines indicate the suspended (supported) segments of a CNF identified through image contrast [13]: (a) Case 1: Au contacts (left) before and (right) after breakdown at the midpoint. (b) Case 2: Near-midpoint breakdown with Au and SiO_2 contacts. (c) Case 3: Breakdown closer to the SiO_2 side with SiO_2 and W–Au contacts. In (b), a suspended segment exists over the electrode region. High-resolution images at a breakdown point were reported in [10].

$a(x)$ to describe heat transport from CNF to its environment (air, substrate, or electrode). The values of $a(x)$ are determined by fitting to experimental data.

We use two types of CNF-electrode contact methods. In the first method, a CNF is placed on Au electrodes, which are about ∼100 nm higher than the SiO_2 surface, using a drop-cast technique. The initial resistance between the electrodes is in the MΩ range, but after several cycles of applied current (current stressing), it decreases to the kΩ range [11]. In the second

Manuscript received January 10, 2009. First published April 14, 2009; current version published April 28, 2009. This work was supported by the U.S. Army Space and Missile Defense Command SMDC and carries Distribution Statement A (approved for public release; distribution unlimited). The review of this letter was arranged by Editor S. Kawamura.

The authors are with the Center for Nanostructures, Santa Clara University, Santa Clara, CA 95053 USA (e-mail: tyamada@scu.edu).

Digital Object Identifier 10.1109/LED.2009.2016361

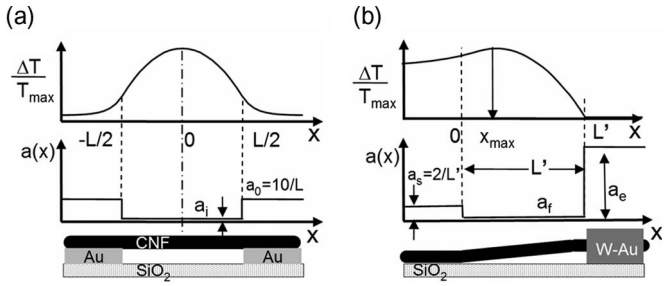

Fig. 3. (a) Model for symmetric contacts with discrete dissipation factors a_i and a_0. The ΔT solution in Section II-A is plotted for $a_0 L = 10 \gg a_i L$. (b) Model for asymmetric contacts with dissipation factors a_s, a_f, and a_e. The ΔT solution in Section II-B is plotted with $a_e L' \gg a_s L' = 2.5\,\mu\text{m}^{-1} \times 0.8\,\mu\text{m} = 2.0 \gg a_f L'$.

method, a CNF is placed on Au electrodes, and then, tungsten (W) is deposited to secure the contact [12]. The total resistance is in the kΩ range, and there is little effect from current stressing. $J_{\max}$ is consistently larger with W–Au contacts than with Au contacts, as shown in Fig. 1.

Breakdown consistently occurs in the suspended region. There are three cases shown in Fig. 2: 1) for $S = 0$, breakdown occurs at or near the midpoint with W–Au contacts or Au contacts; 2) for $0 < S < 1$ with Au and SiO_2 contacts, breakdown occurs near the middle of the suspended segment; and 3) for $0 < S < 1$ with W–Au and SiO_2 contacts, breakdown occurs close to the SiO_2-supported region. SEM images of breakdown are shown in Fig. 2(a)–(c), corresponding to cases 1)–3) earlier.

II. Heat Transport Model

To explain these experimental findings, we solve a 1-D heat transport equation [5], [11], [14]

$$d^2\Delta T(x)/dx^2 - a^2\Delta T = -bJ^2. \tag{1}$$

ΔT is the local CNF temperature at x measured from the ambient temperature. J is the current density, and a is the dissipation factor measuring the effectiveness of heat dissipation to the contact material with unit of inverse length. $b = 1/(\kappa\sigma)$, where κ is the thermal conductivity and σ is the electrical conductivity of the CNF. Heat diffusion (first term) and heat dissipation (second term) generally depend on location, while heat generation (right-hand side) does not. If a is constant, the general solution for (1) is given by $\Delta T = A\cosh(ax) + B\sinh(ax) + bJ^2$, with A and B being constant. Across the interface between two domains with different dissipation factor a, we require ΔT and $d\Delta T/dx$ to be continuous.

A. $J_{\max}$ as a Function of L for Symmetric Contacts

Because of symmetry, we consider only the right half of the CNF. As shown in Fig. 3(a), for the electrode region, $x \geq L/2$, $a(x) = a_0$, and $\Delta T = A_s \exp(-a_0 x) + bJ^2/a_0^2$, while for the region between the electrodes, $0 < x < L/2$, $a(x) = a_i$, and $\Delta T = B_s \cosh(a_i x) + bJ^2/a_i^2$. Since heat dissipation is larger in the electrode region, $R = a_i/a_0 < 1$ holds true. For $J_{\max}$ analysis, a_i is appropriately weighted over the supported and suspended regions in partially supported cases of $0 < S < 1$. Using the boundary conditions at $x = L/2$, we obtain $A_s = a_i F \sinh(a_i L/2)$ and $B_s = -a_0 F$, where $F = bJ^2(1/a_i^2 - 1/a_0^2)/[a_i \sinh(a_i L/2) + a_0 \cosh(a_i L/2)]$, with $\Delta T_{\max}$ occurring at $x = 0$. We assume that CNF breakdown occurs when $\Delta T_{\max}$ reaches the threshold ΔT_{th} [11], which is independent of the CNF length or radius. The maximum current density $J_{\max}$ can then be expressed in terms of a_i, a_0, and L by

$$J_{\max} = \sqrt{\frac{\Delta T_{\text{th}} a_i^2}{b}} \left[1 - \frac{1 - R^2}{R\sinh(a_i L/2) + \cosh(a_i L/2)}\right]^{-1/2}. \tag{2}$$

We consider the following various limits of this expression.

1) Short CNF ($a_i L/2 \ll 1$) with $R \ll a_i L/4 \ll 1$:

$$J_{\max} \sim \sqrt{8\Delta T_{\text{th}}/b}/L. \tag{3}$$

2) Long CNF ($a_i L/2 \gg 1$) with $R \ll 1$:

$$J_{\max} \sim \sqrt{\Delta T_{\text{th}} a_i^2/b}\,[1 + \exp(-a_i L/2)]. \tag{4}$$

3) Short CNF ($a_i L/2 \ll 1$) with any R:

$$J_{\max} \sim \sqrt{\Delta T_{\text{th}} a_i^2/b}\sqrt{8(1 - R^2)/\,[4Ra_i L + (a_i L)^2]}. \tag{5}$$

4) Long CNF ($a_i L/2 \gg 1$) with any R:

$$J_{\max} \sim \sqrt{\Delta T_{\text{th}} a_i^2/b}\,[1 + (1 - R)\exp(-a_i L/2)]. \tag{6}$$

The long-L limit represents the direct balance of heat generation with dissipation to the substrate. The correction for shorter L accounts for the heat dissipated to both the substrate and electrodes. To examine this further, the calculated results for $\Delta T(x)$ and $a(x)$ are shown in Fig. 3(a), which correspond to case 1 in Fig. 2. Limit 1) was discussed in our previous work [11], and limit 3) was reported elsewhere [7].

B. Breakdown Location for Asymmetric Contacts

We consider for the SiO_2 region $x < 0$, $a(x) = a_s$, and $\Delta T = A_a \exp(a_s x) + bJ^2/a_s^2$, for the fully suspended ($S = 0$) region $0 < x < L'$, $a(x) = a_f$, and $\Delta T = B_a \cosh(a_i x) + C_a \sinh(a_f x) + bJ^2/a_f^2$, and for the electrode region $L' < x$, $a(x) = a_e$, and $\Delta T = D_a \exp(-a_e x) + bJ^2/a_e^2$, as shown in Fig. 3(b), where a_s, a_f, and a_e are defined. A_a, B_a, C_a, and D_a are then determined using the boundary conditions at $x = 0$ and L'

$$\begin{aligned}
A_a &= \frac{bJ^2\left(1/a_e^2 - 1/a_f^2\right) - bJ^2\left(1/a_s^2 - 1/a_f^2\right) ch}{(ch + a_s sh/a_f)a_e \exp(a_e L') + a_f sh + a_s} \\
&\quad \times a_e \exp(a_e L') \\
B_a &= bJ^2\left(1/a_s^2 - 1/a_f^2\right) + A_a \\
C_a &= a_s A_a / a_f \\
D_a &= (a_i sh + a_s)A_a / \left[a_e \exp(a_e L')\right]
\end{aligned} \tag{7}$$

where $ch = \cosh(a_f L')$ and $sh = \sinh(a_f L')$. $\Delta T_{\max}$ occurs at $x_{\max} = -a_f^{-1}\tanh^{-1}(C_a/B_a)$. In the limit of very large a_e due to the W–Au electrode, finite a_s due to the SiO_2-supported

region, and negligible a_f in the suspended segment, $\tanh^{-1}$ is expanded, and we obtain

$$x_{\max} \cong \left[1/2 - 1/(a_s L')^2\right] L'. \tag{8}$$

The breakdown location clearly shifts away from the midpoint by $1/(a_s L')^2$ toward the SiO_2-supported region since the heat dissipation in the W–Au region is much more efficient than the SiO_2-supported region. This result is shown in Fig. 3(b), where $\Delta T_{\max}$ shifts away from the W–Au contact with $\Delta T \sim 0$ there and remains finite near the SiO_2-supported region. This prediction is completely consistent with our SEM observations shown in Fig. 2, as discussed hereinafter.

III. Comparison With Experiment

In Fig. 1, there is a straight-line lower bound for the $J_{\max}$ versus $1/L$ behavior, and its gradient is $(8\Delta T_{\rm th}/b)^{1/2} = 54$ kA/m from (3). Thus, $\Delta T_{\rm th} b = \Delta T_{\rm th}\kappa\sigma = 3.4 \times 10^8$ W/$\Omega \cdot$ m^2. We do not have direct measurement results for $\Delta T_{\rm th}$ and κ. For CNFs, a value of $\sigma = 24$ kS/m was reported based on a four-point measurement [8]. Our CNF samples yield $\sigma = 10^4 \sim 10^5$ S/m with an average of 25 kS/m, obtained using the four-point measurement. For CNTs, $\Delta T_{\rm th}$ was estimated to be 600 K in air through a thermogravimetric measurement [15]. $\kappa = 12$ W/m $\cdot$ K was deduced from a thermal resistance measurement using a Pt-coated CNF [16]. If $\Delta T_{\rm th} = 600$ K and $\kappa = 12$ W/m $\cdot$ K are used, then $\sigma = 47$ kS/m, which is double the reported value, as well as our average value, but still within our measured σ range. Fabris *et al.* [14] pointed out that the $\Delta T_{\rm th}\kappa\sigma$ product tends to be overestimated without considering heating at electrode contacts in the model. This would explain our somewhat large $\Delta T_{\rm th}\kappa\sigma$ value extracted from the measurement data in Fig. 1.

From $(8\Delta T_{\rm th}/b)^{1/2} = 54$ kA/m, we deduce the long-L limit for $J_{\max}$, $J_0(a_i) = (\Delta T_{\rm th} a_i^2/b)^{1/2} = 19$ (kA/m) $\times$ a_i (m^{-1}). Fitting this to measurement results in Fig. 1 for $S = 0.69$, 0.81, and 1.0 and using (2) in the limit $R \ll 1$, we obtain $a_i = 2.48$, 1.60, and 1.27 μm^{-1}, with $J_0 = 4.5$, 3.0, and 2.3 MA/cm^2, respectively. As shown in Fig. 1, the resulting calculated $J_{\max}$ behaviors compare well with measurement results for substrate-supported cases.

Breakdown locations in Fig. 3 can be explained by assuming $a \to \infty$ for W–Au contacts, $a \sim 0$ for full suspension, and finite a for Au and SiO_2 contacts. Applying these assumptions for symmetric contacts leads to breakdown location at the midpoint of the suspended segment. This prediction is confirmed by the observations shown in Fig. 2(a) and (b). For case 3 in Fig. 2(c), since the W–Au contact can dissipate heat much more effectively, the breakdown location moves away from the center toward the SiO_2-supported region. In fact, the observed breakdown location $x_{\max}/L'$ in Fig. 2(c) is shifted by $\sim$1/4 from the center toward the substrate contact. Using (8) with $L' \sim 0.8$ μm, we estimate $a_s \sim 2.5$ μm^{-1}. This indicates that the breakdown experiments and the results of the present model can be used for estimation of the heat dissipation factor in these hybrid substrate contact systems. A calculated $\Delta T/T_{\max}$ plot corresponding to these values is shown in Fig. 3(b). ΔT is clearly nonzero in the SiO_2-supported region, and its peak is shifted toward this region away from the W–Au contact. This prediction matches well the observation in Fig. 2(c). Based on this analysis, one can study heat dissipation in similar systems by examining breakdown locations experimentally.

IV. Conclusion

We have developed an analytical heat transfer model that takes into account a piecewise spatially varying heat dissipation factor, and we have successfully explained previous measurements of current capacity and observations of breakdown locations in carbon nanofiber interconnect systems under various electrode and substrate-supported contact conditions.

References

[1] M. Nihei, A. Kawabata, D. Kondo, M. Horibe, S. Sato, and Y. Awano, "Electrical properties of carbon nanotube bundles for future via interconnects," *Jpn. J. Appl. Phys.*, vol. 44, no. 4A, pp. 1626–1628, 2005.

[2] S. Salahuddin, M. Lundstrom, and S. Datta, "Transport effects on signal propagation in quantum wires," *IEEE Trans. Electron Devices*, vol. 52, no. 8, pp. 1734–1742, Aug. 2005.

[3] J. J. Plombon, K. P. O'Brien, F. Gstrein, V. M. Dubin, and Y. Jiao, "High-frequency transport electrical properties of individual and bundled carbon nanotubes," *Appl. Phys. Lett.*, vol. 90, no. 6, p. 063 106, Feb. 2007.

[4] P. J. Burke, "An RF circuit model for carbon nanotubes," *IEEE Trans. Nanotechnol.*, vol. 2, no. 1, pp. 55–58, Mar. 2003.

[5] M. A. Kuroda, A. Cangellaris, and J.-P. Leburton, "Nonlinear transport and heat dissipation in metallic carbon nanotubes," *Phys. Rev. Lett.*, vol. 95, no. 26, p. 266 803, Dec. 2005.

[6] E. Pop, D. Mann, K. Goodson, and H. Dai, "Electrical and thermal transport in metallic single-wall carbon nanotubes on insulating substrates," *J. Appl. Phys.*, vol. 101, no. 9, p. 093 710, May 2007.

[7] C. Durkan, M. A. Schneider, and M. E. Welland, "Analysis of failure mechanisms in electrically stressed Au nanowires," *J. Appl. Phys.*, vol. 86, no. 3, pp. 1280–1286, Aug. 1999.

[8] L. Zhang, D. Austin, V. I. Merkulov, A. V. Meleshko, K. L. Klein, M. A. Guillorn, D. H. Lowndes, and M. L. Simpson, "Four-probe charge transport measurements on individual vertically aligned carbon nanofibers," *Appl. Phys. Lett.*, vol. 84, no. 20, pp. 3972–3974, May 2004.

[9] Q. Ngo, A. M. Cassell, A. J. Austin, J. Li, S. Krishnan, M. Meyyappan, and C. Y. Yang, "Characteristics of aligned carbon nanofibers for interconnect via applications," *IEEE Electron Device Lett.*, vol. 27, no. 4, pp. 221–224, Apr. 2006.

[10] M. Suzuki, Y. Ominami, Q. Ngo, C. Y. Yang, A. Cassell, and J. Li, "Current induced breakdown of carbon nanofibers," *J. Appl. Phys.*, vol. 101, no. 11, p. 114 307, Jun. 2007.

[11] H. Kitsuki, T. Yamada, D. Fabris, J. R. Jameson, P. Wilhite, M. Suzuki, and C. Y. Yang, "Length dependence of current-induced breakdown of carbon nanofibers," *Appl. Phys. Lett.*, vol. 92, no. 17, p. 173 110, Apr. 2008.

[12] T. Saito, T. Yamada, D. Fabris, H. Kitsuki, P. Wilhite, M. Suzuki, and C. Y. Yang, "Improved contact for thermal and electrical transport in carbon nanofiber interconnects," *Appl. Phys. Lett.*, vol. 93, no. 10, p. 102 108, Sep. 2008.

[13] M. Suzuki, T. Yamada, and C. Y. Yang, "Monte Carlo simulation of scanning electron microscopy bright contrast images of suspended carbon nanofibers," *Appl. Phys. Lett.*, vol. 90, no. 8, p. 083 111, Feb. 2007.

[14] D. Fabris, H. Kitsuki, T. Yamada, X. Sun, J. Gonzalez-Cruz, and C. Y. Yang, "Temperature modeling for carbon nanofiber breakdown," in *Proc. ASME Summer Heat Transfer Conf.*, Jacksonville, FL, Aug. 10–14, 2008.

[15] K. Hata, D. N. Futaba, K. Mizuno, T. Namai, M. Yumura, and S. Iijima, "Water-assisted highly efficient synthesis of impurity-free single walled carbon nanotubes," *Science*, vol. 306, no. 5700, pp. 1362–1364, Nov. 2004.

[16] C. Yu, S. Saha, J. Zhou, L. Shi, A. M. Cassell, B. A. Cruden, Q. Ngo, and J. Li, "Thermal contact resistance and thermal conductivity of carbon nanofibers," *J. Heat Transf.*, vol. 128, no. 3, pp. 234–239, Mar. 2004. Carbon nanotubes or films are reported to have orders of magnitude larger κ, attributed to the high crystalline quality.